Synchronization of Micromechanical Oscillators Using Light

Mian Zhang,[1] Gustavo S. Wiederhecker,[1,2] Sasikanth Manipatruni,[1] Arthur Barnard,[3]
Paul McEuen,[3,4] and Michal Lipson[1,4]

[1]*School of Electrical and Computer Engineering, Cornell University, Ithaca, New York 14853, USA*
[2]*Instituto de Física, Universidade Estadual de Campinas, 13083-970 Campinas, SP, Brazil*
[3]*Laboratory of Atomic and Solid State Physics, Cornell University, Ithaca, New York 14853, USA*
[4]*Kavli Institute at Cornell for Nanoscale Science, Ithaca, New York 14853, USA*

Synchronization, the emergence of spontaneous order in coupled systems, is of fundamental importance in both physical and biological systems. We demonstrate the synchronization of two dissimilar silicon nitride micromechanical oscillators, that are spaced apart by a few hundred nanometers and are coupled through an optical cavity radiation field. The tunability of the optical coupling between the oscillators enables one to externally control the dynamics and switch between coupled and individual oscillation states. These results pave a path toward reconfigurable synchronized oscillator networks.

Synchronization processes are part of our daily experiences as they occur widely in nature, for example, in firefly colonies, pacemaker cells in the heart, nervous systems, and circadian cycles [1]. Synchronization is also of great technological interest since it provides the basis for timing, signal processing, and microwave communication [2] and could enable novel computing and memory concepts [3,4]. At the nanoscale, synchronization mechanisms have the potential to be integrated with current nanofabrication capabilities and to enable scaling up to network sizes [5–8]. Among the major challenges with synchronized oscillators on the nanoscale are neighborhood restriction and nonconfigurable coupling which limit the control, the footprint and possible topologies of complex oscillator networks [9–13]. Recently, it is proposed that using cavity field coupled oscillators could form an all-to-all coupling that could overcome this restriction [10,14]. Here we demonstrate the synchronization of two dissimilar silicon nitride (Si_3N_4) self-sustaining optomechanical oscillators coupled only through the optical cavity radiation field as opposed to coupling through a structural contact or electrostatic interaction [15,16]. We externally control the dynamics and switch between coupled and individual oscillation states through tuning the optical coupling between the oscillators. These results pave a path toward realizing massive optomechanical oscillator arrays [17–19].

Optomechanical oscillators (OMOs) consist of cavity structures that support both tightly confined optical modes and long-living (high quality factor) mechanical modes [20,21]. When optomechanical cavities are driven by a blue detuned continuous wave (cw) laser, the radiation pressure from the light can amplify the mechanical motion via the dynamical backaction between the optical and mechanical modes [22]. Above a certain threshold laser power this optomechanical amplification can overcome the intrinsic mechanical damping; the device evolves from an

optomechanical resonator to a self-sustaining OMO [11]. The laser signal fraction that is transmitted, or reflected, from the optomechanical cavity becomes deeply modulated at the mechanical frequency of the oscillator [20,23,24].

Recently it has been predicted that the mechanical oscillations of a pair of OMOs could be synchronized if the OMOs are optically coupled as opposed to mechanically coupled [14,25]. Here we experimentally demonstrate the synchronization of two optically coupled OMOs [right (R) and left (L)] with different mechanical frequencies. The optical coupling means the mechanical displacement of one OMO will lead to a force on the other OMO through the optical field. This force is responsible for the effective
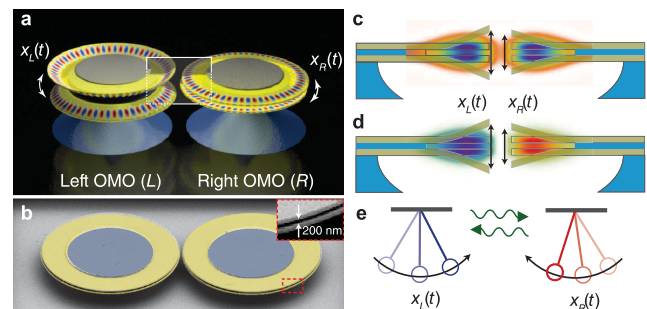

FIG. 1 (color). Design of the optically coupled optomechanical oscillators (OMOs). (a) Schematic of the device illustrating the mechanical mode profile and the optical whispering gallery mode. (b) False-colored scanning electron micrograph (SEM) image of the OMOs with chrome heating pads (blue) for optical tuning by top illumination. (c),(d) The symmetric (S) and antisymmetric (AS) coupled optical supermodes. The deformation illustrates the mechanical mode that is excited by the optical field. (e) The dynamics of the coupled OMOs can be approximated by a lumped model for two optically coupled damped-driven nonlinear harmonic oscillators.

mechanical coupling between the two OMOs. As the OMOs are pumped by a blue-detuned cw laser into self-sustaining oscillations, the R (L) OMO not only experiences the oscillation at its natural frequency but also a modulated optical force at the L (R) OMO's mechanical frequency. As the coupling between the two oscillators is increased, each OMO is eventually forced to oscillate at an intermediate frequency between their natural frequencies (Ω_R and Ω_L), that is, the onset of synchronization [14,26,27]. We observe both the individual freerunning and synchronized oscillation dynamics by switching on and off the purely optical coupling between two OMOs.

Each individual OMO consists of two suspended vertically stacked Si$_3$N$_4$ disks, where the optical and mechanical modes of such a cavity are localized around the OMO's freestanding edge [Figs. 1(a) and 1(b)]. The disks are fabricated using standard electron-beam lithography followed by dry and wet etching steps (see the Supplemental Material [28]). The two disks are 40 μm in diameter and 210 nm in thickness, while the air gap between them is 190 nm wide. Such a small gap and the relative low refractive index of Si$_3$N$_4$ ($n \approx 2.0$) induce a strong optical coupling between the top and bottom disks. The resonant frequency of the optical modes of the stacked disks depend strongly on their separation [29]; therefore any mechanical vibration that modulates the vertical gap width also modulates the optical resonant frequency; a measure for the efficiency of this process is the optomechanical coupling, defined as $g_{\rm om} = \partial\omega/\partial x$, where ω is the optical frequency and x is the mechanical mode amplitude [20,29,30]. Our device exhibits a large optomechanical coupling rate, calculated to be $g_{\rm om}/2\pi = 49$ GHz/nm (see the Supplemental Material [28]). The mechanical mode that couples most strongly to the optical field is also illustrated by the deformation of the disks edge in Figs. 1(a), 1(c), and 1(d) which has a natural frequency of $\Omega_m/2\pi \approx 50.5$ MHz. Note that the two cavities are not identical and without the optical coupling they oscillate at different mechanical frequencies.

The two OMOs are separated by a distance of $d_g = (400 \pm 20)$ nm, minimizing direct mechanical coupling. This gap results in evanescent optical coupling between the OMOs when their optical resonant frequencies are close. The optical coupling leads to two optical supermodes spatially spanning both OMOs: a symmetric, lower frequency mode $b_+(t)$ [Fig. 1(c)] and an antisymmetric higher frequency mode $b_-(t)$ [Fig. 1(d)]. Their eigenfrequencies are given by $\omega_\pm = \bar\omega \pm \kappa/2$, where $\bar\omega = (\omega_L + \omega_R)/2$ and ω_L (ω_R) is the uncoupled optical resonant frequency of the L (R) OMO and κ is the optical coupling rate: a reflection of the distance between the two cavities. The mechanical modes of each cavity can be approximated by a lumped model consisting of two damped harmonic oscillators, which are driven by the nonlinear optical supermode forces,

$$\ddot{x}_j + \Gamma_j \dot{x}_j + \Omega_j^2 x_i = F_{\rm opt}^{(j)}(x_R, x_L)/m_{\rm eff}^{(j)}, \quad \text{for} \quad j, k = L, R,$$
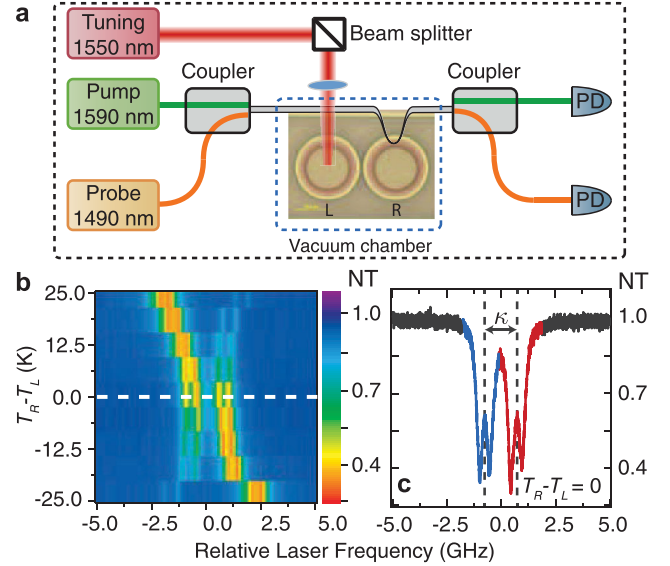

FIG. 2 (color).   Controlling the OMO system. (a) Schematic of the experimental setup. The pump and probe light are launched together into the cavities and are detected separately by photodiodes (PD). (b) Anticrossing of the optical mode as the relative temperature of the L OMO (T_L) and the R OMO (T_R) is changed through varying the tuning laser power. The tuning laser is focused on to the two OMOs respectively to obtain the negative and positive relative temperatures. (c) Transmission spectrum of the maximally coupled state indicated by the white horizontal line in (b). S (blue) and AS (red) optical supermodes with optical coupling rate κ. NT: normalized transmission.

where x_j, Ω_j, Γ_j, and $m_{\rm eff}^{(j)}$ represent the mechanical displacement, mechanical resonant frequency, dissipation rate, and effective motional mass of each mechanical degree of freedom. The optical force is proportional to the optical energy stored in the coupled optical modes, which depend both on x_R and x_L, i.e., $F_{\rm opt}^{(j)}(x_R, x_L) \propto |b_\pm(x_R, x_L)|^2$. Therefore, the optical field not only drives but also mechanically couples each OMO. The nonlinear nature of this driving and coupling force form the basis for the onset of synchronization. In a first order linear approximation when the two OMOs are evenly coupled ($\omega_L = \omega_R$), the effective mechanical coupling force between the two oscillators is given by $F_{\rm coup}^{(i)} = -k_I x_j + k_Q \dot{x}_j$, where k_I and k_Q are the position and velocity coupling coefficients (see the Supplemental Material [28]). In the unresolved side band limit (optical damping rate $\gamma \ll \Omega_j$), these coupling coefficients are determined by both the input optical power $P_{\rm in}$ and laser-cavity detuning Δ as $k_I \propto P_{\rm in}\Delta[(\gamma/2)^2 + \Delta^2]^{-2}$ and $k_Q \propto P_{\rm in}(\gamma/2)\Delta[(\gamma/2)^2 + \Delta^2]^{-3}$. Therefore, by varying Δ and $P_{\rm in}$, hence the effective mechanical coupling strength, synchronization of the two OMOs can be captured.

We experimentally demonstrate that the system can be reconfigured to exhibit either coupled or single OMO dynamics by controlling the optical mode coupling
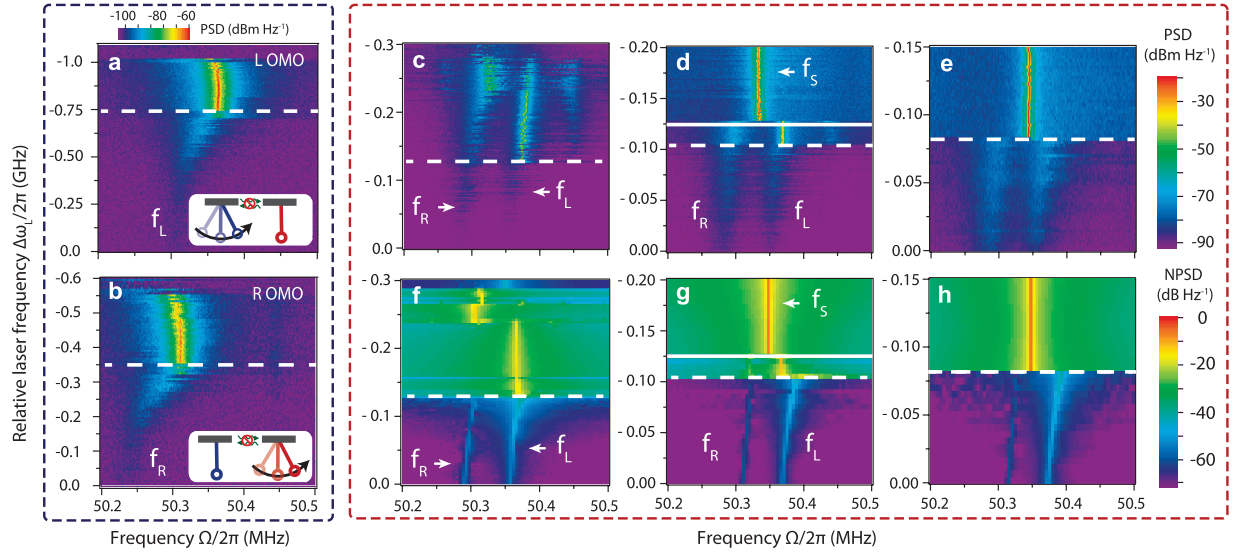
FIG. 3 (color).   rf spectra of the OMOs and synchronization (a), (b) rf power spectra of cavity L (a) and R (b) as a function of laser frequency when the coupling is turned off. The horizontal white lines indicate the onset of self-sustaining oscillation. Power spectral density (PSD). (c) When the coupling is turned on, at an input power $P_{\text{in}} = (1.8 \pm 0.2)$ μW cavities L and R do not synchronize and oscillate close to their natural frequencies. (d) At $P_{\text{in}} = (11 \pm 1)$ μW synchronization occurs after the horizontal solid white line after a brief region of unsynchronized oscillation (between the dashed and solid white lines). (e) The system oscillate directly in a synchronized state at input optical power $P_{\text{in}} = (14 \pm 1)$ μW. (f), (g), (h) Corresponding numerical simulations for the OMO system based on the lumped harmonic oscillator model described in the text. Normalized power spectral density (NPSD).

between the two oscillators. While the distance between the two OMOs is fixed (i.e., fixed κ), their optical coupling can be turned off (on) through increasing (decreasing) the optical frequency mismatch $\delta = \omega_R - \omega_L$ between them. For large optical frequency mismatch among the two OMOs ($\delta \gg \kappa$) the supermodes reduce to the uncoupled optical modes of the individual OMO, $(b_+, b_-) \rightarrow (a_L, a_R)$. This can be readily seen from the expression of the optical supermodes amplitudes, which are given by linear combinations of the uncoupled modes of the left $a_L(t)$ and right $a_R(t)$ cavities: $b_{\pm}(t) = a_L(t) - a_R(t)i\kappa/(\delta \mp (\delta^2 - \kappa^2)^{1/2})$. We tune δ experimentally using the thermo-optic effect, for which the optical frequency dependence on temperature can be approximated as $\omega_j(T_j) = \omega_0^{(j)} - g_{\text{th}}T_j$ for $j = L, R$, where $\omega_0^{(j)}$ is the intrinsic optical frequency and gth is the thermal-optic tuning efficiency. The thermo-optic tuning is accomplished by focusing an out-of-plane heating laser on either OMO (Fig. 2(a); see the Supplemental Material [28]). This setup allows the optical coupling to be continuously tuned through changing the relative temperature of the two OMOs: at $\Delta T = 0$ the OMOs have identical optical resonant frequencies and the optical coupling is maximized, manifested by the almost symmetric resonance dips in the optical transmission spectrum [Figs. 2(b) and 2(c)], whereas for $\Delta T = \pm 25$ K, the relative frequency difference is large ($\delta \gg \kappa$) and the optical mode does not couple the two OMOs. The OMOs follow the usual single-cavity optomechanical dynamics [20].

We characterize the individual dynamics of the two OMOs by switching their optical coupling off [$T = \pm 25$ K, Fig. 2(b)]. Each cavity is individually excited with a cw laser through a tapered optical fiber. As the laser frequency is tuned (from a higher to a lower frequency) into the optical resonance, the transmitted laser signal is detected by a photodiode (PD) and analyzed using a radio-frequency spectrum analyzer (RSA). The rf spectra show the mechanical modes have natural mechanical frequencies of $(f_L, f_R) = (\Omega_L, \Omega_R)/2\pi = (50.283, 50.219)$ MHz, and intrinsic quality factors of $(Q_m^{(L)}, Q_m^{(R)}) = (3.4 \pm 0.3, 2.3 \pm 0.2) \times 10^3$ [Figs. 3(a) and 3(b)]. Because of the increased optomechanical backaction and intracavity optical power the OMOs have their frequencies increased (optical spring effect) and amplitudes grown as the laser is tuned into the optical resonance. Above a specific laser-cavity detuning, indicated by the horizontal white dashed lines on Figs. 3(a) and 3(b) the intrinsic mechanical losses are completely suppressed by the optomechanical amplification. At this point the optomechanical resonator starts self-sustaining oscillations and becomes an OMO characterized by sudden linewidth narrowing and oscillation amplitude growth [10,11,14]. It is clear from Figs. 3(a) and 3(b) that each cavity has only one mechanical mode in the frequency range of interest. Because of the slight difference in geometry, these frequencies differ by $\Delta f = f_L - f_R = (70.0 \pm 0.5)$ kHz.

We show the onset of spontaneous synchronization by switching their optical coupling on. Using the heating laser,
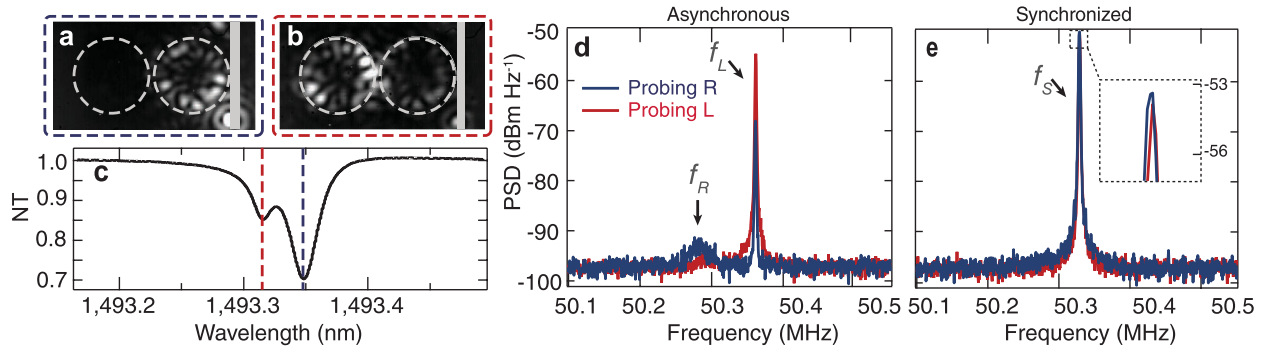
FIG. 4 (color). Pump-probe measurements of the oscillations of individual OMO operating as in Fig. 3(d). (a), (b) The uneven probe intensity distribution of the cavities, observed by an infrared CCD camera when the pump laser is off. (c) Normalized transmission (NT) spectrum for the probe resonances. The red (blue) dashed line corresponds to the probe wavelength region for probing the L (R) OMO, as illustrated in (a), (b). (d) The red (blue) curve is the L (R) cavity probe transmission rf spectrum when the two OMOs are asynchronous: a strong peak at f_L is observed but with very different amplitude for two probing conditions. (e) Same curves shown in (d) but with the OMOs synchronized: the two probing conditions have almost identical amplitudes.

we tune the optical coupling to its maximum value, indicated by the dashed white line ($T_R - T_L = 0$) in Fig. 2(b). The laser frequency sweeping is performed at various optical power levels corresponding to different effective mechanical coupling strength. The optical power ranges from slightly above the estimated oscillation threshold (i.e., weaker mechanical coupling), $P_{\text{th}}^{(L,R)} \approx (640, 880)$ nW, up to several times their threshold power (i.e., stronger mechanical coupling). At a relative low input power, $P_{\text{in}} = (1.8 \pm 0.2)$ μW, the mechanical peaks at f_R and f_L are simultaneously observed on the rf spectrum shown in Fig. 3(c), below the dashed-white line. When the laser frequency is closer to the optical resonant frequency, more energy is available and the L OMO starts self-sustaining oscillation. Since cavity R has a higher oscillation threshold, due to its lower mechanical quality factor, it requires more optical power and only oscillates at a redder detuning; it can be noticed from Fig. 3(c) that both OMOs oscillate close to their natural frequency. Therefore they exhibit asynchronous oscillations at this lowest power level. At a higher input optical power level of $P_{\text{in}} = (11 \pm 1)$ μW, the first oscillation takes place at $\Delta\omega_L/2\pi \approx -0.10$ GHz, and similarly to the case shown in Fig. 3(c), the L OMO oscillates first. However, as the laser frequency further moves into the optical resonance, there is enough energy for both OMOs to start self-sustaining oscillations; the two OMOs spontaneously oscillate in unison at an intermediate frequency of $f_S = \Omega_S/2\pi = 50.37$ MHz due to the increased effective mechanical coupling, which is a clear sign of synchronization. At this time, the output optical rf power is increase by more than 5 dB in comparison with the L OMO oscillating only case showing that the two OMOs are phase locked. At an even higher optical input power, $P_{\text{in}} = (14 \pm 1)$ μW, the OMOs do not oscillate individually, instead they go directly into synchronized oscillations above the white dashed line in Fig. 3(e). We confirm that the OMOs are

indeed synchronized by performing numerical simulations corresponding to each of the power levels we tested. The simulated spectra in Figs. 3(f)–3(h) exhibit all the essential features observed and show good agreement with the measured spectra. It also allows us to confirm under which conditions the two OMOs are indeed oscillating (see the Supplemental Material [28]).

To experimentally verify that both structures are indeed oscillating at the synchronized frequency, we probe the mechanical oscillation of each cavity individually. This demonstrates that the single oscillation peaks observed in Figs. 3(d) and 3(e) are not caused by one OMO resonantly driving the other; it also verifies that amplitude death of one of the OMOs does not occur, a known phenomenon in coupled nonlinear oscillators [31]. We used a weak cw probe laser to excite an optical resonant mode that is not strongly coupled between the two OMOs [Figs. 2(a) and 2(b)]; this scheme allows us to selectively probe the oscillations of the L or R OMO. While these probe optical modes exhibit a low optical quality factor ($Q_{\text{opt}} \approx 4 \times 10^4$) that minimizes probe-induced perturbations to the mechanical oscillations, the pump condition is identical to the one used in Fig. 3(d). When the L OMO is probed, and the pump detuning range is between the dashed and solid lines in Fig. 3(d), the probe rf spectrum shows a strong peak at f_L, which is shown in the red curve in Fig. 4(d). When the R OMO is probed, a peak also appears at this frequency, but it is 13 dB weaker as shown in the blue curve in Fig. 4(d); a weak peak at f_R can also be noticed on the blue curve, indicating small amplitude oscillations of the R OMO. These results confirm that the oscillation state is very asynchronous in this detuning range with the L OMO oscillating at much larger amplitude. When the pump laser detuning is above the horizontal solid line in Fig. 3(d) there is only a single rf peak at the synchronized frequency f_S when probing either OMO [Fig. 4(e)]; moreover, they differ in amplitude by less than 0.5 dB. This shows that both cavities

are indeed oscillating with similar strength at the synchronized frequency.

We have demonstrated the onset of synchronization between two optomechanical oscillators coupled only through the optical radiation field. The ability to control the coupling strength is promising for realizing oscillator networks in which the oscillators can be addressed individually. Furthermore, established and future microphotonics techniques such as electro-optic and thermo-optic techniques can now be extended to switch, filter, and phase shift the coupling of these oscillators. These results may enable a new class of devices in sensing, signal processing and on-chip nonlinear dynamical systems.

[1] S. H. Strogatz, *Sync: The Emerging Science of Spontaneous Order* (Hyperion, New York, 2003), 1st ed.

[2] S. Bregni, *Synchronization of Digital Telecommunications Networks* (Wiley, Chichester, 2002).

[3] I. Mahboob and H. Yamaguchi, Nat. Nanotechnol. **3**, 275 (2008).

[4] M. Bagheri, M. Poot, M. Li, W. P. H. Pernice, and H. X. Tang, Nat. Nanotechnol. **6**, 726 (2011).

[5] S. Kaka, M. R. Pufall, W. H. Rippard, T. J. Silva, S. E. Russek, and J. A. Katine, Nature (London) **437**, 389 (2005).

[6] F. Mancoff, N. Rizzo, B. Engel, and S. Tehrani, Nature (London) **437**, 393 (2005).

[7] S.-B. Shim, M. Imboden, and P. Mohanty, Science **316**, 95 (2007).

[8] M. Zalalutdinov, K. Aubin, M. Pandey, A. Zehnder, R. Rand, H. Craighead, J. Parpia, and B. Houston, Appl. Phys. Lett. **83**, 3281 (2003).

[9] D. J. Watts and S. H. Strogatz, Nature (London) **393**, 440 (1998).

[10] G. Heinrich, M. Ludwig, J. Qian, B. Kubala, and F. Marquardt, Phys. Rev. Lett. **107**, 043603 (2011).

[11] F. Marquardt, J. G. E. Harris, and S. M. Girvin, Phys. Rev. Lett. **96**, 103901 (2006).

[12] F. Marquardt, Nature (London) **478**, 47 (2011).

[13] J. L. Arlett, E. B. Myers, and M. L. Roukes, Nat. Nanotechnol. **6**, 203 (2011).

[14] C. A. Holmes, C. P. Meaney, and G. J. Milburn, Phys. Rev. E **85**, 066203 (2012).

[15] E. Buks and M. Roukes, J. Microelectromech. Syst. **11**, 802 (2002).

[16] R. B. Karabalin, M. C. Cross, and M. L. Roukes, Phys. Rev. B **79**, 165309 (2009).

[17] F. Massel, S. U. Cho, J.-M. Pirkkalainen, P. J. Hakonen, T. T. Heikkilä, and M. A. Sillanpää, Nat. Commun. **3**, 987 (2012).

[18] M. Ludwig and F. Marquardt, arXiv:1208.0327.

[19] A. Tomadin, S. Diehl, M. D. Lukin, P. Rabl, and P. Zoller, Phys. Rev. A **86**, 033821 (2012).

[20] T. Kippenberg and K. Vahala, Opt. Express **15**, 17172 (2007).

[21] V. Braginsky, S. Strigin, and S. Vyatchanin, Phys. Lett. A **287**, 331 (2001).

[22] T. J. Kippenberg and K. J. Vahala, Science **321**, 1172 (2008).

[23] T. Carmon, H. Rokhsari, L. Yang, T. J. Kippenberg, and K. J. Vahala, Phys. Rev. Lett. **94**, 223902 (2005).

[24] I. S. Grudinin, H. Lee, O. Painter, and K. J. Vahala, Phys. Rev. Lett. **104**, 083901 (2010).

[25] S. Manipatruni, G. Wiederhecker, and M. Lipson, in *Proceedings of the Quantum Electronics and Laser Science Conference* (Optical Society of America, Rochester, NY, 2011), p. QWI1.

[26] M. Cross, A. Zumdieck, R. Lifshitz, and J. Rogers, Phys. Rev. Lett. **93**, 224101 (2004).

[27] M. Hossein-Zadeh and K. Vahala, Appl. Phys. Lett. **93**, 191115 (2008).

[28] See Supplemental Material at http://link.aps.org/supplemental/10.1103/PhysRevLett.109.233906 for additional information on theoretical modeling and data analysis.

[29] G. S. Wiederhecker, L. Chen, A. Gondarenko, and M. Lipson, Nature (London) **462**, 633 (2009).

[30] G. S. Wiederhecker, S. Manipatruni, S. Lee, and M. Lipson, Opt. Express **19**, 2782 (2011).

[31] R. Mirollo and S. Strogatz, J. Stat. Phys. **60**, 245 (1990).